Engineering Tunability through Electro-optic Effects to Manifest Multifunctional Metadevice

Taimoor Naeem[1], Hafiz Saad Khaliq[1], Muhammad Zubair [1], Tauseef Tauqeer [1*], Muhammad Qasim Mehmood[1*]

[1]NanoTech Lab, Department of Electrical Engineering, Information Technology University (ITU) of the Punjab, 4th floor Arfa Software Technology Park, Ferozepur Road, Lahore 54600, Pakistan

Supporting Information

Note 1:

In anisotropic media, electric flux density is related to electric field by following relation

$$D_j = \sum_{ij} \varepsilon_{ij} E_j \qquad \text{i,j = x,y,z components} \tag{1}$$

Expanding the above equation will result in nine independent permittivity coefficients. However, matter tensors usually possess symmetry property ($\varepsilon_{ij} = \varepsilon_{ji}$), and the coefficients are reduced to diagonalized form as

$$\begin{pmatrix} \varepsilon_{xx} & 0 & 0 \\ 0 & \varepsilon_{yy} & 0 \\ 0 & 0 & \varepsilon_{zz} \end{pmatrix} \tag{2}$$

This kind of tensor may be represented by quadric expression by

$$\sum_{ij} \varepsilon_{ij} x_i x_j = 1 \tag{3}$$

It depicts that E and D are parallel for the principle plane and axis. Furthermore, anisotropic material refractive indices are not the tensor components, but they are related to principal components of impermeability tensor η, which is given by

$$\eta = \varepsilon_0 \varepsilon^{-1} = 1/n^2 \tag{4}$$

where n is refractive index of the material. By expanding Eq. 2

$$\eta_{xx}x^2 + \eta_{yy}y^2 + \eta_{zz}z^2 + \eta_{yz}yz + \eta_{zy}zy + \eta_{xy}xy + \eta_{yx}yx + \eta_{zx}zx + \eta_{xz}xz = 1 \tag{5}$$

$$\eta_{xx}x^2 + \eta_{yy}y^2 + \eta_{zz}z^2 + 2\eta_{yz}yz + 2\eta_{xy}xy + 2\eta_{xz}xz = 1 \tag{6}$$

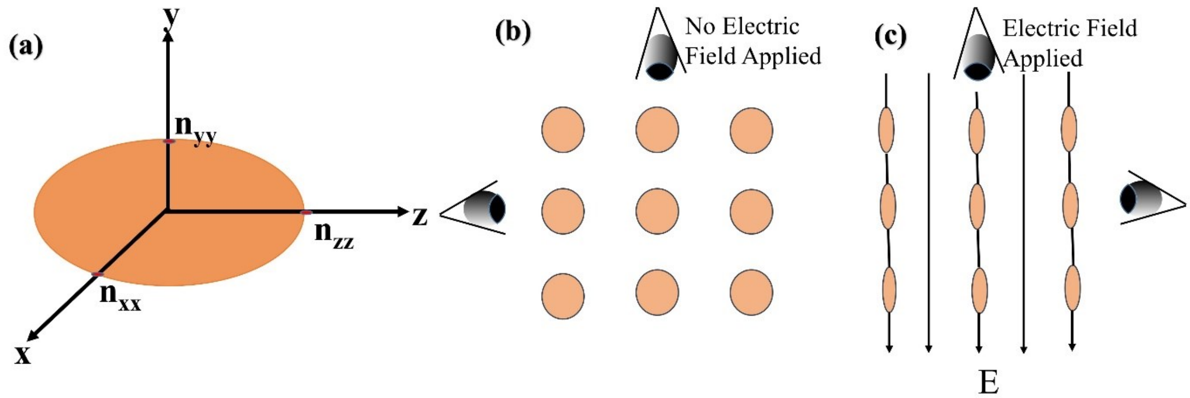

Fig. S1: (a) Ordinary and extraordinary axis. (b) Electrons from a different perspective when the no-electric field is applied. (c) Electrons variation from different perspective under applied electric field results in birefringence

Since the tensor is symmetric which transform it in terms of the principal axis

$$\eta_{xx}x^2 + \eta_{yy}y^2 + \eta_{zz}z^2 = 1 \tag{7}$$

When compared it with the standard ellipse equation, we get three principal axes as η_{xx} , $\eta_{yy,}$ and $\eta_{zz,}$ which are the three axes of the ellipsoid as shown in Fig. 2(a). These are the essential aspect of understanding the light wave traveling in any birefringent material. The extent of medium symmetry can be analyzed if $\eta_{xx} = \eta_{yy} = \eta_{zz}$ the medium will be considered as isotropic, as shown in Fig. 2(b). However, if $\eta_{xx} = \eta_{yy} \neq \eta_{zz}$ the medium will be uniaxial, two refractive indexes which are equal, is known as the ordinary refractive index. The third one is the extraordinary refractive index, as shown in Fig 2(c). If the electric field is applied at the material, change in impermeability tensor will be given as

$$\delta\eta = r_{ijk}E_k \tag{8}$$

Where r_{ijk_k} is the electro-optic coefficient and third rank tensor, which has 27 independent elements. Due to symmetric constraints, these elements are reduced since i,j reduced to six elements in Eq. 7, so we can replace i,j by k, which has six coefficients, reducing the matrix dimensions to 6x3. Since $\eta_l = 1/n_l^2$ we get

$\delta n_l = -0.5n^3\delta\eta_l$ put this in Eq. 9.

$$\delta n_l = -0.5n^3 r_{lk} E_k \tag{9}$$

Also, E=V/d, where d is the thickness of the EO layer. In the case of BTO, the applied electric field will vary the refractive index, as shown in Fig. 3(d), where r_{51} =1300 pmV^{-1} and n = 2.4 under no applied electric field. The phase of the optical diffractive element varies with the applied electric field by the following relation.

$$\varphi(E) = \phi_o - \frac{\pi}{\lambda} r n_o^3 E.l \tag{10}$$

where l is the height of the slab.

Note 2:

For spatial phase profile of the zoom lens to demonstrate focusing at different points, each row should exhibit different phase. To get this, phase profile accompanied by metasurface should follow hyperboloidal profile given by:

$$\varphi(r) = -\frac{2\pi}{\lambda}\left(\sqrt{x^2 + f^2} - f\right) \tag{11}$$

where f is the distance between the centre of the lens to the focal point, x is the distance of the row from lens centre.

The dynamic zooming for the three wavelengths of 488 nm, 532 nm, and 633 nm is illustrated in the Fig. S2, Fig. S3 and Fig. S4. The voltage distribution for focusing at f=25 µm, f=30 µm, f=35 µm and f=40 µm is presented in Fig. S2(a-d) and corresponding phase distribution is illustrated in Fig. S2(e-h) given by (11). Fig. S2 (i-l) shows the focusing at different points by apply acquired voltage distributions to corresponding pixels. Fig S3 shows voltage distribution (a-d) and phase distribution (e-h) at wavelength of 532 nm for different focus points. Fig. S4 demonstrate the voltage distribution, phase profile and dynamic zooming for the 633 nm wavelength.

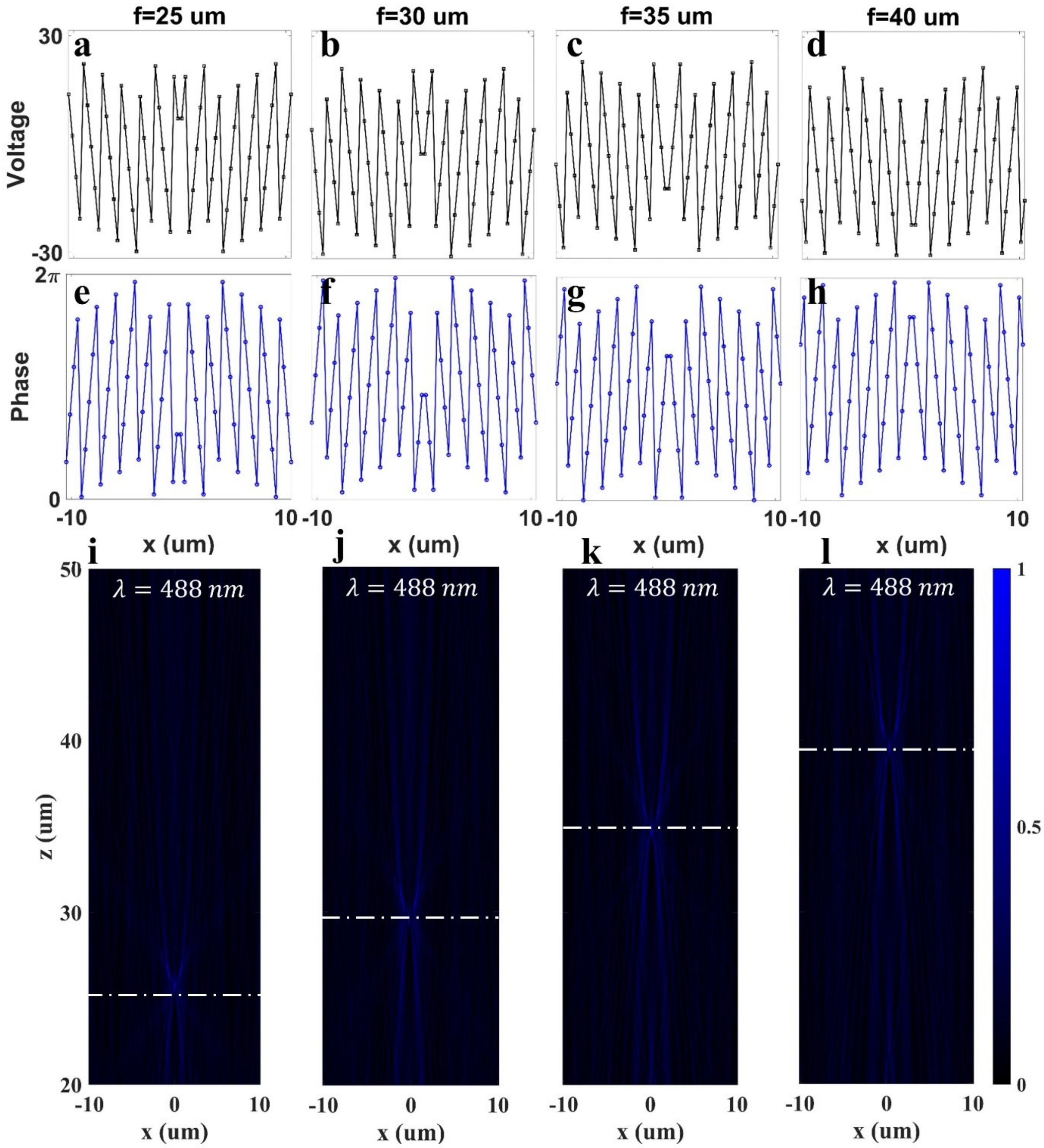

Fig. S2: Voltage distribution for focusing at (a) 25 μm, (b) 30 μm, (c) 35 μm and (d) 40 μm for wavelength at 488 nm. (e-h) shows corresponding phase distribution for focusing at (25 to 40) μm. Full wave simulation of $|E|^2$ for focusing at (25 to 40) μm is illustrated in (i-l) respectively.

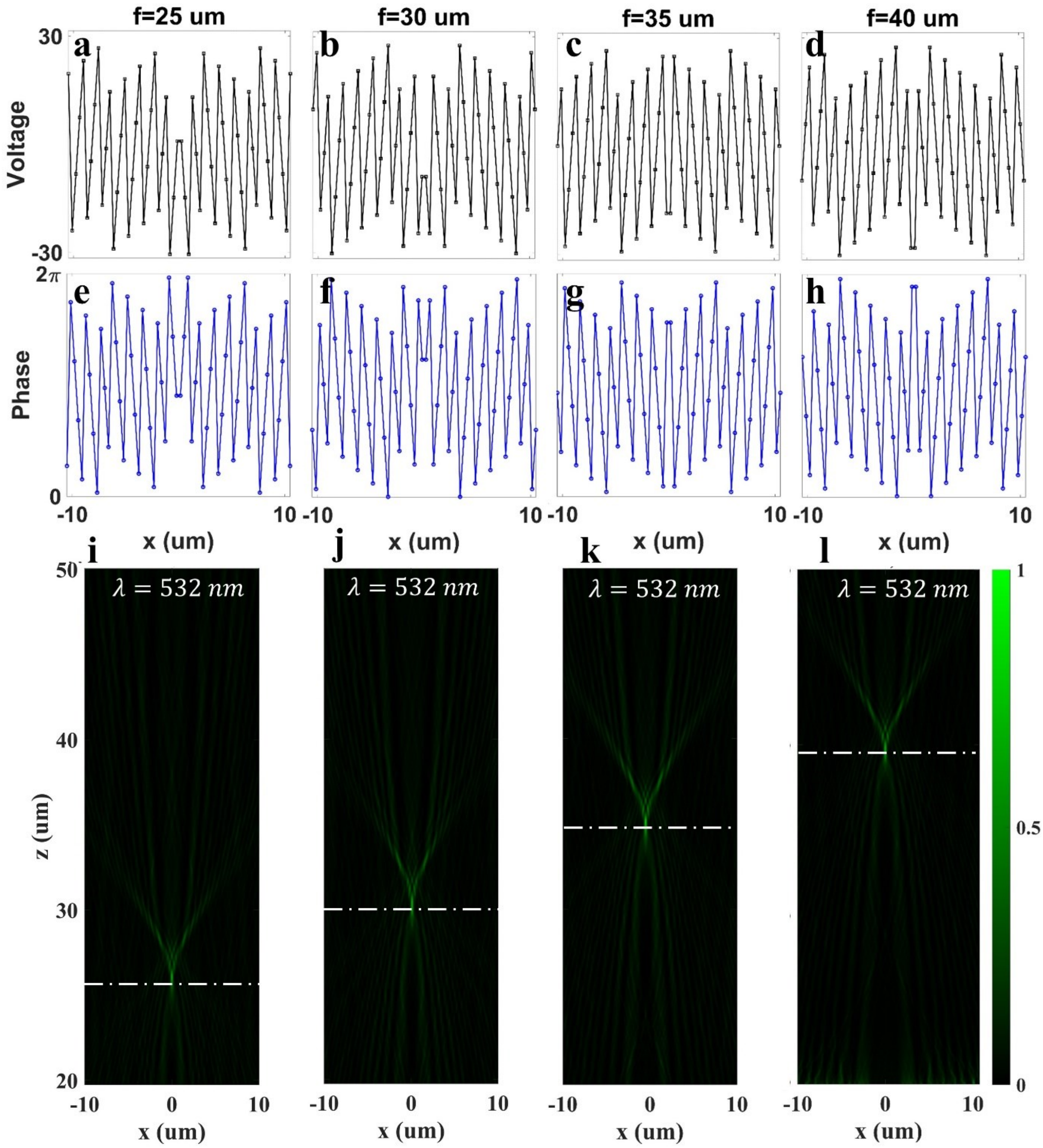

Fig. S3: Voltage distribution for focusing at (a) 25 μm, (b) 30 μm, (c) 35 μm and (d) 40 μm for wavelength at 488 nm. (e-h) shows corresponding phase distribution for focusing at (25 to 40) μm. Full wave simulation of |E|2 for focusing at (25 to 40) μm is illustrated in (i-l) respectively.

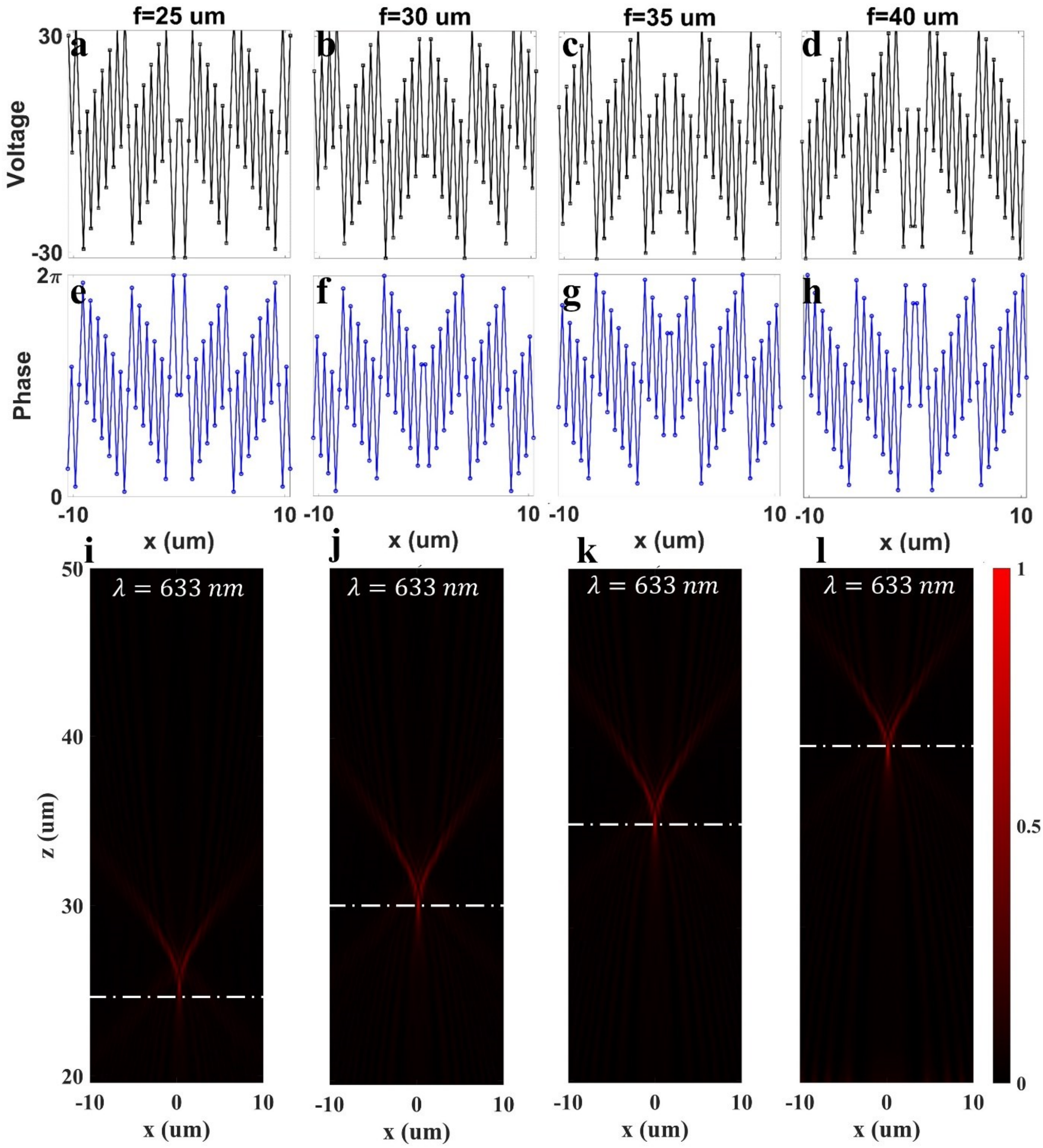

Fig. S4: Voltage distribution for focusing at (a) 25 μm, (b) 30 μm, (c) 35 μm and (d) 40 μm for wavelength at 488 nm. (e-h) shows corresponding phase distribution for focusing at (25 to 40) μm. Full wave simulation of |E|2 for focusing at (25 to 40) μm is illustrated in (i-l) respectively.